ISSN 1726-5749

SENSORS & TRANSDUCERS

2 vol. 10 Special /11

Sensor Device Technologies and Applications

International Frequency Sensor Association Publishing

IFSA

Sensors & Transducers

Volume 10, Special Issue, February 2011 | www.sensorsportal.com | ISSN 1726-5479

Sensors & Transducers Journal

Contents

Volume 10
Special Issue
February 2011

www.sensorsportal.com

ISSN 1726-5479

Research Articles

Authors are encouraged to submit article in MS Word (doc) and Acrobat (pdf) formats by e-mail: editor@sensorsportal.com
Please visit journal’s webpage with preparation instructions: http://www.sensorsportal.com/HTML/DIGEST/Submition.htm

International Frequency Sensor Association (IFSA).

The Second International Conference on Sensor Device Technologies and Applications

SENSORDEVICES 2011

August 21-27, 2011 - French Riviera, France

IFSA
www.sensorsportal.com

Important deadlines:

Submission deadline	March 23, 2011
Notification	April 30, 2011
Registration	May 15, 2011
Camera ready	May 22, 2011

Tracks:
- Sensor devices
- Photonics
- Infrared
- Ultrasonic and Piezosensors
- Sensor device technologies
- Sensors signal conditioning and interfacing circuits
- Medical devices and sensors applications
- Sensors domain-oriented devices, technologies, and applications
- Sensor-based localization and tracking technologies

http://www.iaria.org/conferences2011/SENSORDEVICES11.html

The Fifth International Conference on Sensor Technologies and Applications

SENSORCOMM 2011

August 21-27, 2011 - French Riviera, France

IFSA
www.sensorsportal.com

Important deadlines:

Submission deadline	March 23, 2011
Notification	April 30, 2011
Registration	May 15, 2011
Camera ready	May 22, 2011

Tracks:
- APASN: Architectures, protocols and algorithms of sensor networks
- MECSN: Energy, management and control of sensor networks
- RASQOFT: Resource allocation, services, QoS and fault tolerance in sensor networks
- PESMOSN: Performance, simulation and modelling of sensor networks
- SEMOSN: Security and monitoring of sensor networks
- SECSED: Sensor circuits and sensor devices
- RIWISN: Radio issues in wireless sensor networks
- SAPSN: Software, applications and programming of sensor networks
- DAIPSN: Data allocation and information in sensor networks
- DISN: Deployments and implementations of sensor networks
- UNWAT: Under water sensors and systems
- ENOPT: Energy optimization in wireless sensor networks

http://www.iaria.org/conferences2011/SENSORCOMM11.html

The Fourth International Conference on Advances in Circuits, Electronics and Micro-electronics

CENICS 2011

August 21-27, 2011 - French Riviera, France

IFSA
www.sensorsportal.com

Important deadlines:

Submission deadline	March 23, 2011
Notification	April 30, 2011
Registration	May 15, 2011
Camera ready	May 22, 2011

Tracks:
- Semiconductors and applications
- Design, models and languages
- Signal processing circuits
- Arithmetic computational circuits
- Microelectronics
- Electronics technologies
- Special circuits
- Consumer electronics
- Application-oriented electronics

http://www.iaria.org/conferences2011/CENICS11.html

Sensors & Transducers Journal, Vol. 10, Special Issue, February 2011, pp. 60-70

www.sensorsportal.com

Sensors & Transducers

ISSN 1726-5479

http://www.sensorsportal.com

Charge-sensitive Infrared Phototransisotrs: Single-photon Detctors in the Long-Wavelength Infrared

[1]Takeji Ueda and [2]Susumu Komiyama
Department of Basic Science, the University of Tokyo
Komaba 3-8-1, Meguro-ku, Tokyo, 153-8902, Japan
Fax/Tel.: +81-3-5454-6960
E-mail: ueda@iis.u-tokyo.ac.jp

Received: 18 October 2010 /Accepted: 11 January 2011 /Published: 8 February 2011

Abstract: Novel ultrasensitive detectors in the wavelength range of λ = 5-50 μm have developed. The detectors are *charge-sensitive infrared phototransistors* (CSIPs) fabricated in GaAs/AlGaAs double quantum well structures. The devices serve as a phototransistor capable of counting single photons, while a function is similarly to CMOS image sensors. The excellent noise equivalent power (NEP = $6.8\cdot10^{-19}$ W/Hz$^{1/2}$) and specific detectivity (D^* = $1.2\cdot10^{15}$ cmHz$^{1/2}$/W) are demonstrated for λ = 14.7 μm, which are by a few orders of magnitude superior to those of the other state-of-the-art detectors. These figures of merit persist up to 23K. Temperature dependence of the performance is studied and wavelength range expansion is attempted. The simple planar structure of CSIPs is feasible for array fabrication including future monolithic integration with reading circuits. *Copyright © 2011 IFSA.*

Keywords: THz, Single-photon detector, Ultrasensitive, Temperature dependence, Wavelength range expansion.

1. Introduction

Far Infrared range (FIR, the wavelength range of λ=15-300 μm) and terahertz range (THz, λ =100-1000 μm) cover very wide spectral region compared to rather limited visible region (λ =0.3-0.7 μm). This vast spectral range, however, is now a frontier of science and technology [1-3], while the shorter and the longer spectral ranges have been extensively explored by optics and electrical engineering. The FIR-THz range provides an expanding research field of interdisciplinary science and technology [1-3], where wide-spread different areas meet and give impetus to each other. The relevant areas include physics [4], electronics [5, 6], optics [7], chemistry [8], biology [9, 10], medicine [11], astronomy [12], environmentology [13], spectroscopy [7-10], imaging [4, 11, 12], security [14] and communication [15].

From the viewpoint of spectroscopy, the most remarkable feature of the FIR-THz range is the rich spectra of matters. This made possible firm identification of solid, molecules and chemical bondings through *fingerprint* like spectra. Another important feature of the FIR-THz radiation is that it is thermally emitted by every material at room temperature [1].This made FIR-THz radiation a unique tool for studying temperature distribution of matters and internal activity of the objects. Familiar application includes night vision, thermography, and astronomical observation. The combination of these – spectroscopy of spontaneous emission– can be a powerful method for studyng *living* bio-systems. One may observe inside biocells without touching, killing or modulating their natural active states. For detecting such extremely weak local emission, the passive microscopy requires ultra-sensitive detectors reaching photon-counting level.

Differently from routinely used photon-counters in near-infrared or visible range, FIR-THz photon-counters are limited to semiconductor quantum devices, which are still under development [16-18]. A series of THz detectors in wavelength range of 100 μm - 1 mm have been realized by combining a quantum dot (QD) with a single electron transistor (SET) [16-18]. The detectors are applied to passive microscopy of electron systems [19-21] as well as to implementation of on-chip device [22], in which single THz photons are generated, propagated and counted. The application of these detectors to passive microscopy to room temperature object is, however, restricted because they need ultra-low temperatures (<1 K). In this sense, shorter wavelength (5-50 μm) may be attractive because detectors can be designed for higher temperature operation.

In this paper, we describe novel ultra-sensitive detectors of 5-50 μm range developed by utilizing a double-quantum-well (DQW) structure [23-29]. The detectors are called charge-sensitive infrared phototransistors (CSIPs). We demonstrated single-photon detection as well as ultra-broad dynamic range (>10^6, from attowatts to beyond picowatts [27]). CSIPs can be operated reasonable temperatures (~25 K at 15 μm, depending on wavelength) [28]. The excellent noise equivalent power (NEP=$6.8\cdot10^{-19}$ W/Hz$^{1/2}$) and specific detectivity (D^*=$1.2\cdot10^{15}$cmHz$^{1/2}$/W) are demonstrated for λ=14.7 μm, which are by a few orders of magnitude superior to those of the other state-of-the-art detectors. In addition, the simple planer structure is, similarly to CMOS sensors, feasible for array fabrication and will even make it possible to monolithically integrate with reading circuit.

2. Detection Mechanism and Device Structure

In CSIPs, an electrically isolated island of a QW is photoexcited to serve as a gate to a remote two-dimensional electron gas (2DEG) conducting channel. As schematically shown in Fig. 1 (a), photoexcited electrons escape the isolated QW island leaving holes behind. The photo electrons are driven to the 2DEG conducting channel yielding photocurrens. Another effect larger than this direct photocurrent arises from the positive charge left on the QW island, which, through capacitive coupling, increases the electron density in the 2DEG channel and thus its conductance. The effect persists until the excited electrons recombine with holes in the isolated island, serving as an amplification mechanism. CSIPs are thus charge-sensitive phototransistor, in which a QW island works as a photosensitive floating gate.

The upper QW is so designed that the energy spacing between the ground subband and the first excited subband is ΔE =84 meV (wavelength of λ=15 μm). When radiation with photon energy of ΔE is incident on the isolated QW, electrons are excited to the first excited subband, where the thin tunnel barrier layer stands as schematically depicted in Fig. 2 (b). The electrons, having tunneled out of the QW, fall down the electrostatic potential slope in the graded barrier layer until they eventually reach the 2DEG channel to be absorbed there. This causes isolated QW island to be positively charged. Through capacitive coupling, the pile-up positive charge in the isolated island increases the electron density of the lower 2DEG channel leading to an increase in conductance.

To realize the scheme in the above, we fabricate devices (for a detection-wavelength of 15 μm) in a GaAs/AlGaAs modulation doped heterostructure crystal containing a GaAs QW and an inverse heterostructure as showing in Fig. 1 (c) [23]. The layers are grown by molecular-beam epitaxy on semi-insulating GaAs substrate: They consist of a 1μm thick buffer layer ($Al_{0.3}Ga_{0.7}As$ 20 nm /GaAs 2 nm superlattices), a Si doped ($1\cdot10^{18}$ cm^{-3}) 10-nm $Al_{0.3}Ga_{0.7}As$ electron-supply layer, a 30 nm $Al_{0.3}Ga_{0.7}As$ spacer layer, a 50 nm GaAs lower QW layer, a 100 nm composition graded $Al_xGa_{1-x}As$ ($x=0.01 \rightarrow 0.1$) barrier layer, a 2 nm $Al_{0.2}Ga_{0.8}As$ tunnel barrier, a 10 nm GaAs upper QW layer, a 20 nm $Al_{0.3}Ga_{0.7}As$ spacer layer, a Si doped (1×10^{18} cm^{-3}) 60-nm $Al_{0.3}Ga_{0.7}As$ layer, and a 10 nm GaAs cap layer. For detecting radiation of around λ=30μm, the triangular barrier- upper QW region of crystal structure above is substituted by a 100 nm $Al_xGa_{1-x}As$ graded barrier with $x=0 \rightarrow 0.035$, 2 nm $Al_{0.15}Ga_{0.85}As$ tunnel barrier, the Si-doped ($2.5\cdot10^{17}$ cm^{-3}) GaAs upper QW with the thickness of 17 nm. Typical electron density, N_s, and mobility, μ, are around $N_s = 3\cdot10^{11}$ cm^{-2} and $\mu=3\times10^4$ cm^2/Vs (for undoped QWs) or 100 cm^2/Vs (for doped QWs), respectively.

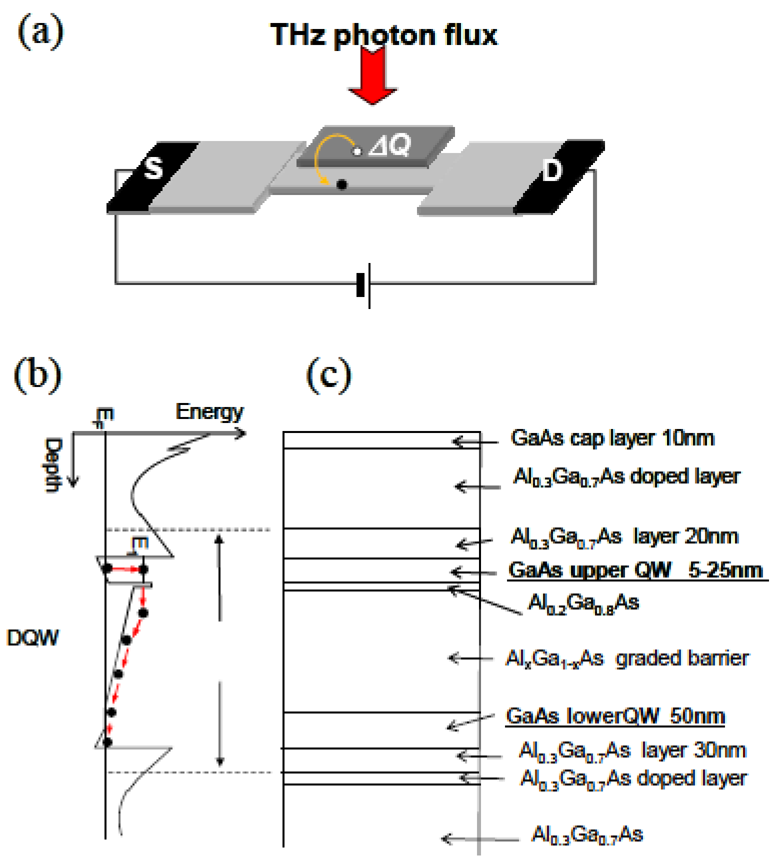

Fig. 1. (a) Schematic representation of a CSIP as a photo-active FET ; (b) The energy diagram of DQW system; (c) Crystal structure for λ=15 μm.

As shown in Fig. 2 (a), the device consists of a wet-etched DQW mesa, alloyed AuGeNi ohmic contacts, Au/Ti Schottky gates (the isolation gate and reset gate), and Au/Ti photo-coupler (antenna). The device is fabricated with standard electron-beam lithography technique. The two dimensional electron gas (2DEG) layer in the both of the QWs are normally connected by ohmic contacts, and can be electrically isolated by biasing metal isolation gates as shown in Fig. 2 (b) where 2DEG layers are illustrated as blue planes. The antenna is used to cause intersubband transition by generating electric filed normal to the plane of the QW against the normally incident radiation. In actual practice of operation, the optimized metal-gate bias is found in gate-bias-dependent IV curve where photosignal reaches maximum amplitude as shown in Fig. 2 (c). The signal appears when FET is formed: upper QW is electrically isolated and the accumulated photoholes induce larger current flowing in the lower QW. The increasing slope for a time-trace of photo-induced current is proportional to a given photon flux as shown in the next section. The active areas of devices are freely defined in lithography. In Fig. 2 (a) and (b), the finger isolation gate is used to form series of floating gates with graded chemical potential witch allows more uniform capacitive coupling over the conducting channel even at the larger source-drain bias voltage for larger signal. The effect of source- drain bias and the size to the unit photon signal amplitude is mentioned in the next section.

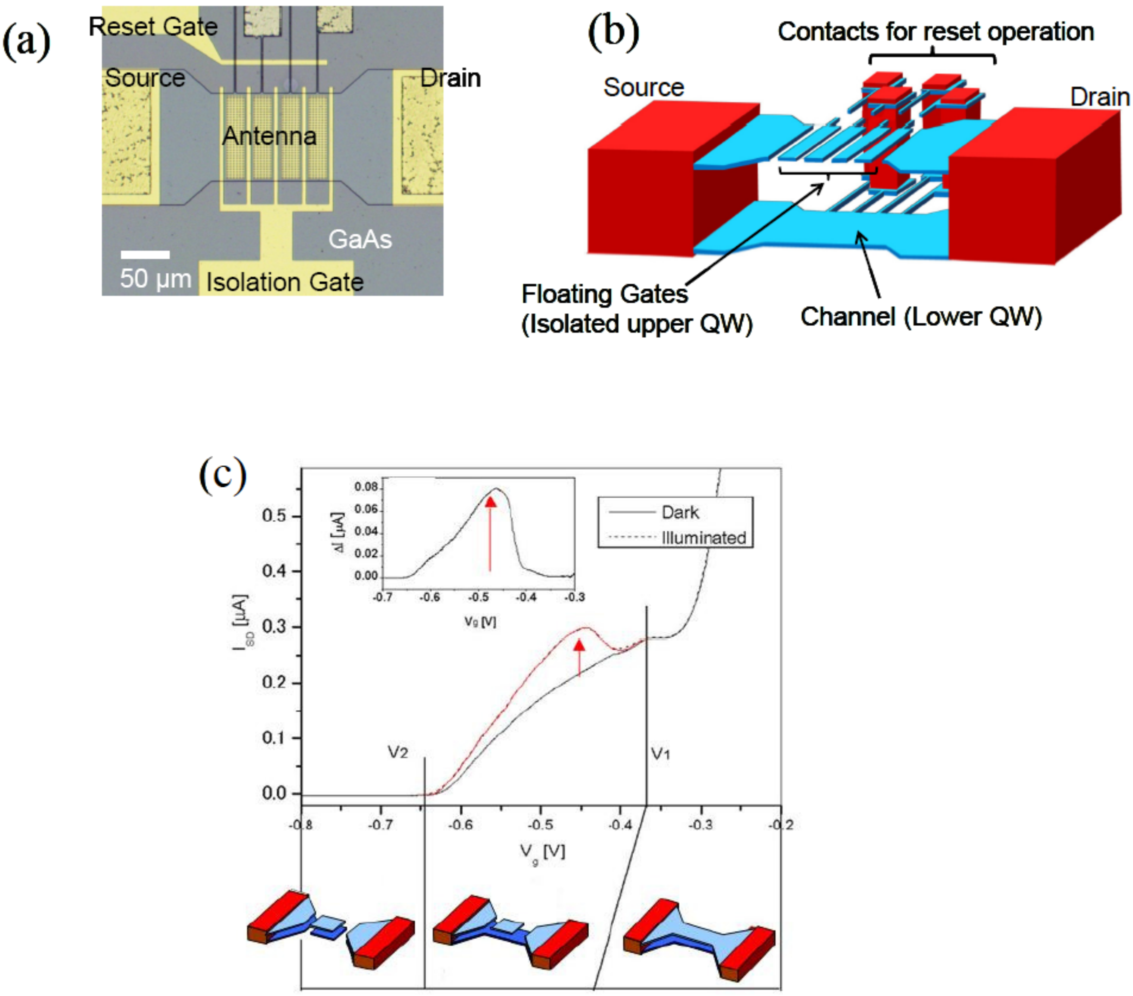

Fig. 2. (a) A microscope image of the device of 150 × 130 μm^2; (b) Schematic representation of QWs and ohmic contacts. The upper QW is electrically isolated by negative biasing of surface gates; (c) *I-V* measurements of a CSIP with scanning gate bias V_G. Photo signal appears under illumination when floating gate is formed.

3. Device Performance

Fig. 3 (a) shows the time-trace of photo-signal for different photon fluxes taken at 4.2 K with source-drain bias voltage of V_{SD}=10 mV after applied reset pulse at t =0 s [26, 27]. The homemade all-cryogenic spectrometer is used for the measurement [27]. The system consists of a reliable

Joule-heating blackbody emitter, a parabolic mirror collimeter, a monochrometer made by gear-controlled rotating diffraction grating, and a CSIP. The whole spectrometer system is immersed in liquid helium, and shielded against background radiation of warmer (T=50 K-300 K) part of the cryostat. The upper QW of the CSIP is isolated with a gate bias of V_G=-0.48 V and the reset pulse of 1μs duration is applied to one of the metal gates. The increase of photo-induced current is extremely slow for all the curves because the incident photon flux applied here is extremely weak. Fig. 3 (b) shows that the spectral response lies at wavelengths around λ=15 μm, where the data is taken by studying the slope $\alpha=\Delta I/\Delta t$ of photo-current increase as a function of the incident radiation wavelength (angle of the diffraction grating).

In the limit of weak radiation, stepwise increase is noted as shown in Fig. 3(c) [25, 27]. This stepwise signal is successfully interpreted by assuming the increase of lower channel electron density, ΔN_s, is equal to the density of photoholes in upper QW, p / LW, where p is the number of photoholes and L is the length of active area along the channel, and W is the width of active area across the channel. The relationship $j=\sigma\varepsilon$ with the increase of two-dimensional current density, $j=\Delta I/W$, the electric field by source-drain bias voltage, $\varepsilon=V_{SD}/L$, and the phohole-modulated two-dimensional transconductivity, σ=e$\mu\Delta N_s$, gives [25, 27].

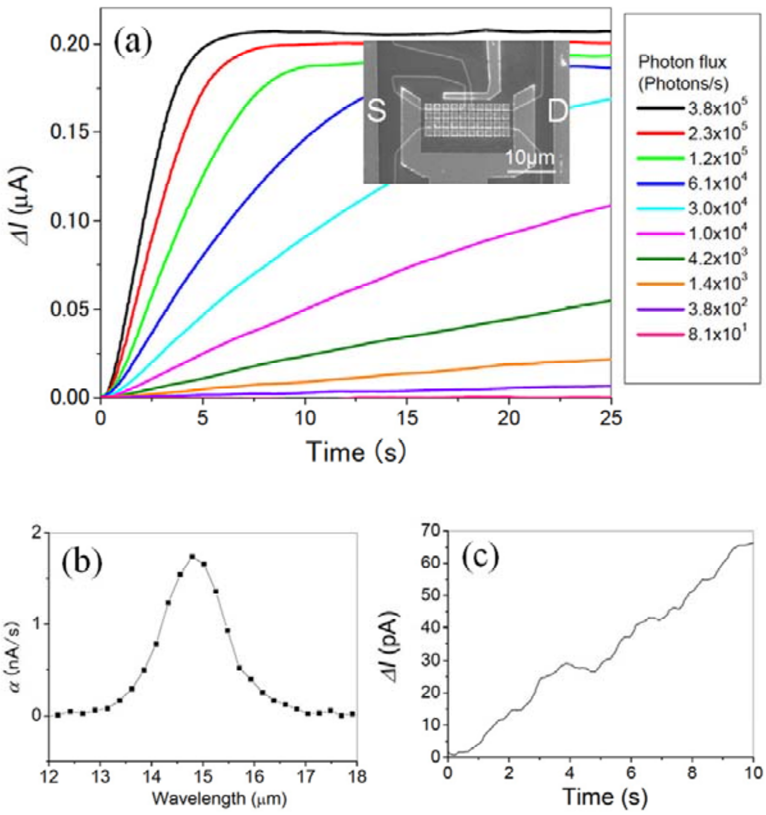

Fig. 3. (a) Time traces of the photo current ΔI obtained with different incident photon fluxes and a SEM micrograph of the device with an active area of 16 × 4 μm^2. (b) The detection spectrogram. (c) Magnified time traces taken with the lowest photon flux (BBR emitter at 50K).

$$\Delta I = \frac{e\mu V_{SD}}{L^2} p = I_e p \, , \tag{1}$$

where I_e is the unit increment of current due to one photohole. The observed step amplitudes for $L \times W$=16 × 4 μm^2 device, ΔI_{SETP}= 3 pA substantially corresponds to the expected single-photon signal,

I_e=2.8 pA by (1). Obviously, smaller device with small L produces larger unit signal -clearer steps- as demonstrated in [25]. It should be noted that in proper detection condition, the lifetime of a photohole is longer than the measurement period by which the slope $\alpha=\Delta I/\Delta t$ of photo-current is proportional to photon flux Φ. When the measurement period is longer than the lifetime, the increase of ΔI levels off as shown in the flat region of time-traces in Fig. 3(a). Therefore in the actual practice of the operation, reset frequency is tuned so that the detector produces only linear responses in a given photon flux range. The photo-current saturation mechanism will be discussed in the next section.

By using (1), the photon-count-rate (α/I_e) can be replotted from Fig. 3 (a) as a function of Φ (Fig. 4) [27]. By heating the BBR emitter from T=50 to 250 K, Φ increases from a level of 3×10/sec to 1×10^8/sec. The dynamic range of detection exceeds 10^6 in the measurement, but the true dynamic range may be higher since the highest photon flux is restricted by the emitter in the measurements. The quantum efficiency is directly determined to be η=2 %. Resent improvement of quantum efficiency to be 7 % will be discussed in Sec. V [29].

Considering the dark count rate of Γ=0.5 s^{-1}, we determine the noise equivalent power of $NEP = h\nu (2\Gamma)^{1/2} / \eta = 6.8\times10^{-19}$ W/Hz$^{1/2}$, and the specific detectivity of $D^* = (WL)^{1/2} / NEP = 2\times10^{15}$ cm Hz$^{1/2}$ /W for the integration time of 1 s [27]. These values may be by a few orders of magnitude better than any other devices reported in the 15 micron wavelength region, e.g. $D^*=10^{12}$ cm Hz$^{1/2}$ /W is one of the best value reported for QWIPs (quantum-well infrared photo-detectors) operated at T=4.2 K [30].

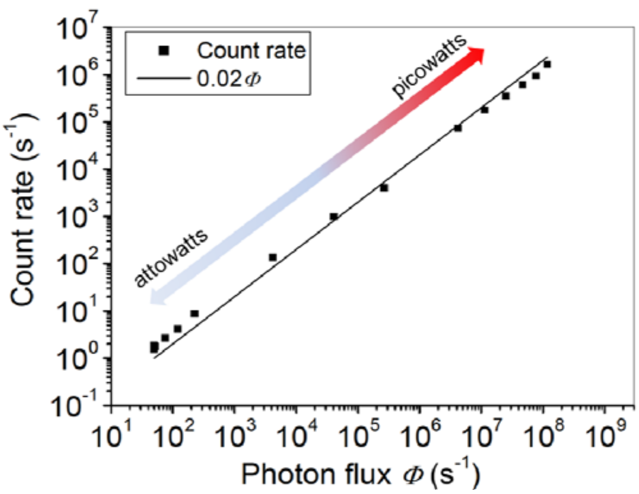

Fig. 4. Count rate of the photo signal vs. photon flux Φ.

The value of D^* for CSIP is much higher than 300K-photon-noise limited performance, which will meet the requirements for high-resolution real-time passive imaging of RT small objects, e.g., living bio-cells. Recently CSIPs have been applied to the construction of a highly sensitive passive microscope [31, 32].

4. Temperature Dependence of the Performance

Higher temperature operation is desired for practical applications. There is in general, however, a trade-off between high sensitivity of an IR detector and operation temperature. The external constraint is that sensitive devices are saturated by strong background blackbody radiation from surrounding materials. The internal constraint is that the thermionic emission inside the device becomes equivalent to photo-emission. The former may be determined by optical setup, as well as relative intensity of signal radiation to the background. Here, we discuss the latter intrinsic constraint.

In Fig. 5, time traces of photo-current at different temperatures are displayed under the fixed photon flux $\Phi=1\times10^5$ s^{-1}[28]. The temperature effect appears as the lower amplitude of photo-current saturation. It should be noted that the slope, $\alpha=\Delta I/\Delta t=\eta\Phi I_e$, in the initial stage of each trace is independent of T, assuring that ηI_e is independent of T. This means higher frequency reset operation is required, i.e., the integration time is shortened, in the elevated temperatures. The photo-signal is discernible up to 30K for the CSIP of λ= 15 µm. The derived NEP and D^* up to T=23 K with integration time of 1s are given as $NEP=8.3\times10^{-19}$ W/Hz$^{1/2}$, and $D^*=9.6\times10^{14}$ cm Hz$^{1/2}$ /W [28], which are not very different from the 4.2 K values mentioned above.

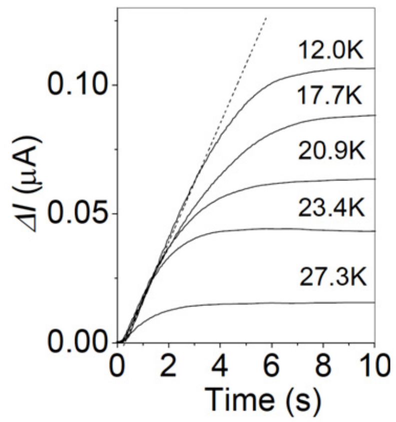

Fig. 5. Time traces of the photocurrent with $\Phi=1\times10^5$ s^{-1} at different temperatures.

The understanding of photo-current saturation directly leads to temperature dependent physics inside the device. The potential profile changing in the detection is shown in Fig. 6. The potential height of the triangular barrier in equilibrium is $U=\Delta E-\delta U$, i.e., barrier hight is lower, by $\delta U\approx15$ meV, than subband energy splitting of ΔE. Here the barrier hight $U=U_U=U_L$ is measured from electrochemical potential of upper or lower QW, $\zeta=\zeta_L=\zeta_U$.

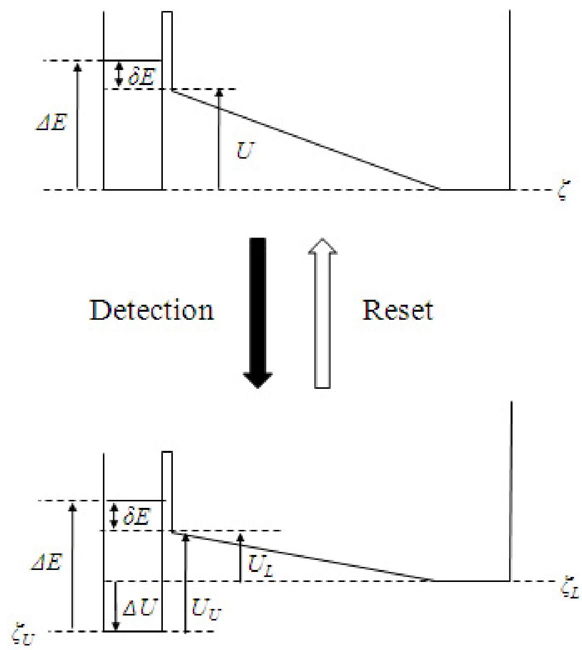

Fig. 6. Energy diagram illustrating photo-saturation. Upper diagram: the chemical potential of two QWs.

Under illumination, the energy of the floating upper QW with p photoholes decreases against the grounded lower QW by $\Delta U = |\zeta_L - \zeta_U| = pe^2 d / \kappa LW$, where d is the distance between the upper and the lower QWs, and $\kappa = 12 \times (8.85 \times 10^{-12})$ F/m is the electronic permittivity of the crystal. The net potential barrier height measured from ζ_L , then decreases to be $U_L = (\Delta E - \delta E) - \Delta U$ by p photoholes, while $U_U = \Delta E - \delta E$ remains constant [24, 31]. The barrier reduction assists the electrons in the lower QW to recombine with photoholes in the upper QW. The photo-current saturation occurs when the recombination process becomes equivalent to the photohole generation process. Obviously, more electrons in the lower QW contribute to the recombination process at higher temperature. Finally at around T=30 K, the number of traveling electron across the barrier exceeds that of photo-emitted electrons even with no band-deformation.

The number of photoholes is determined by a rate equation [28]:

$$\frac{dp}{dt} = \eta\Phi - \frac{p}{\tau} = \eta\Phi + (n_U - n_L), \tag{2}$$

where τ is the lifetime of photholes. The recombination rate, p/τ, is the given by difference between the rate from the upper QW to the lower QW, n_U, and the rate of the opposite flow, n_L. The thermionic electron emission rate from each QW [28] is given by $n=(LW/d)D\int(v\Theta f)dE$, where $D=m^*/\pi\hbar^2$ is the two-dimensional density of states with $m^*=0.0665 \times (9.1 \times 10^{-31})$ kg the effective mass of conduction electrons in GaAs, and $v=(2E/m^*)^{1/2}$ the electron velocity with energy E measured from each ζ, Θ is the transmission probability, and $f= [1+\exp(E/k_BT)]^{-1}$ is the Fermi distribution function with k_B the Boltzmann constant. Equations (1) and (2) can be used to derive lifetime and whole shape of time traces as demonstrated in [28]. Here we derive an expression of temperature limit as a function of subbband energy.

At the temperature limit, T_{lim}, (2) becomes $2\eta\Phi=n_L$,by assuming $\eta\Phi\approx n_U$ under dp/dt=0 and ΔU=0. The relationship between subband energy the ΔE and temperature limit T_{lim} can be obtained:

$$\Delta E - \delta E \approx -k_B T_{\lim} \ln\left(\frac{2\eta\Phi d}{LWDvk_B T_{\lim}}\right) = \gamma T_{\lim}, \tag{3}$$

where $v=(2E_F/m^*)^{1/2}$ is Fermi velocity. Here, integration is made only for $E > U$ with Θ=1 and $f\approx\exp(-E/k_BT)$, i.e., only thermionic emission is considered. Since contribution of T_{lim} in the logarithm is not significant, the temperature limit shows almost linear dependence on the subband energy with quasi-constant γ >0. For the λ=15 μm, the parameter values yields T_{lim} =29 K, which is close to the experimentally observed limit temperature.

5. Wavelength Range Expansion

The detection wavelength is controlled by using different thickness of upper QW layer. Detection of 30 μm wavelength radiation has successfully realized without difficulty as shown in Fig. 7. It is also possible in principle to detect radiation of longer wavelength λ >40 μm and shorter wavelength λ <8 μm. Both direction of wavelength expansion, however, may require higher-level crystal growth technology. In case of λ >40 μm, much lower triangular barrier should be used (U<31 meV), and therefore higher quality of crystal is needed to avoid impurity-oriented potential fluctuation. In case of λ <10 μm, better interface morphology, as well as high quality, is required to form reliable narrow QW (<7 nm) with sufficient electron density. Our recent results for 45 μm will be published elsewhere. Realization of CSIP's detection scheme with different material system, as well as with modified band profiles, or with different excitation mechanism, may be promising for wider wavelength-range expansion.

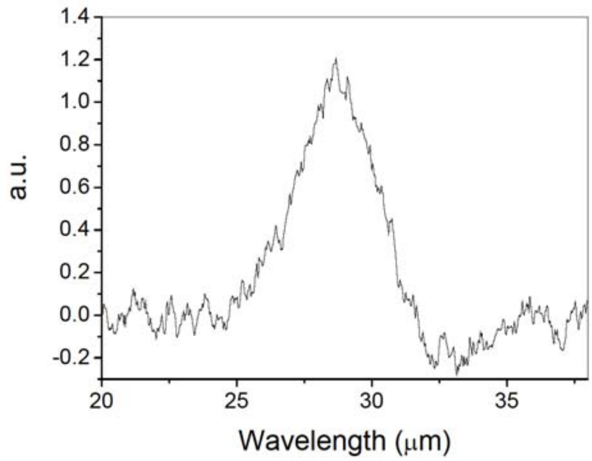

Fig. 7. Spectrogram for a CSIP with a 17 nm-thick upper QW.

Optimization of photo-coupler, the key component determining quantum efficiency, is also important for designing a CSIP for a given target wavelength. Since a CSIP has only one QW for detection which lies at a depth of 100 nm beneath the surface, the photo-coupler geometries used in QWIPs , in which more than 30 QW layers lie in a depth of 0.5-2 μm, cannot be directly applied to CSIPs. Recently we proposed and demonstrated efficient photo-couplers for CSIPs (λ=15 μm) by exploiting surface-plasmon-polariton (SPP) resonance occurring in aperture metal sheets coated on top of the crystal surface (Fig. 8 (a)) [29]. The SPP resonance induces wavelength-selective strong electric confined near the surface of the metal sheets intensifying the subband transition in the QW 100 nm below the surface. After checking the detection wavelength by monochlometer, CSIPs with different coupler were examined under well controlled blackbody emitter (Fig. 2 (b)). Cross-shaped hole arrays, as shown in Fig. (2c), yield the highest efficiency of η=7 %, which is by a factor four higher than that of the square-metal-pad arrays.

By matching two resonance system (coupler and subband in a QW), one can design a CSIP for target wavelength. Development of multi-color CSIPs will be one of the interesting and fruitful works in the future.

6. Conclusion

We developed novel ultrasensitive detectors in a wavelength range of 5-50 μm. To our knowledge, single-photon detection is first achieved in this range. The accurately determined figures of merit are a few order magnitudes superior to other detectors. CSIPs are featured by not only ultra-high sensitivity, but also by versatile applicability due to higher temperature operation as well as extremely wide dynamic range. The simple planar structure is feasible for array fabrication including future monolithic integration with reading circuit.

Acknowledgements

This work is supported by the CREST project of Japan Science and Technology Agency (JST). This article is based on the collaborating work with a number of researchers. Prticularly T. Ueda thanks Z. An, P. Nickels, Z. Wang, N. Nagai and S. Matsuda.

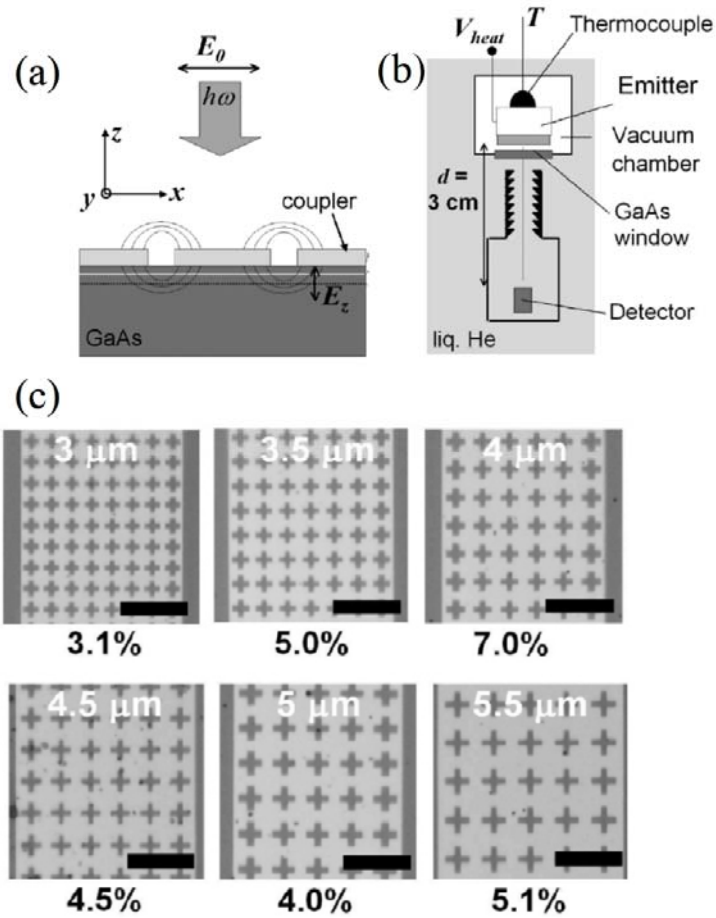

Fig. 8. (a) Schematic representation of the photo coupler; (b) Experimental setup by quantum efficiency; (c) Metal mesh couplers. The period is marked in each micrograph. The scale bar indicates 10 µm. Numbers below each structure are the experimentally derived values of the quantum efficiency η.

References

[1]. Rogalski, and K. Charzanowski, Infrared devices and techniques, *Opto. Electron. Rev.,* Vol. 10, No. 2, 2002, pp. 111-136.

[2]. P. E. Siegel, Terahertz technology, *IEEE Trans. Microwave Theory Tech,*. Vol. 50, No. 3, 2002, pp. 910-928.

[3]. M. Tonouchi, Cutting-edge terahertz technology, *Nat. Photonics*, 1, Feb. 2007, pp. 97-105.

[4]. K. Ikushima, H. Sakuma, S. Komiyama, and K. Hirakawa, Imaging of cyclotron emission from edge channels in quantum Hall conductors, *Phys. Rev. Lett.,* Vol. 93, No. 14, Oct. 2004, pp. 146804.

[5]. T. J. Yen, W. J. Padilla, N. Fang, D. C. Vier, D. R. Smith, J. B. Pendry, D. N. Basov, and X. Zhang, Terahertz magnetic response from artificial materials, *Science*, Vol. 5, No. 5663, 2004, pp. 1494-1496.

[6]. Q. Hu and J. L. Reno, Operation of terahertz quantum-cascade lasers at 164 K in pulsed mode and at 117K in continuous-wave mode, *Optics Express*, Vol. 13, Issue 9, 2005, pp. 3331-3339.

[7]. D. Grischkowsky, S. Keiding, M. Exter, and C. Fattinger, Far infrared time-domain spectroscopy with terahertz beams of dielectric and semiconductors, *J. Opt. Soc. Am. B*, Vol. 7, No. 10, 1990, pp. 2006-2015.

[8]. M. C. Beard, G. M. Turner, and C. A. Schmuttenmaer, Terahertz Spectroscopy, *J. Phys. Chem. B*., Vol. 106, No. 29, 2002, pp. 7146-7159.

[9]. M. Nagel, M. Först, and H. Kurtz, THz biosensing devices: fundamentals and technology, *J. Phys. Condens. Matter,* Vol. 18, Apr. 2006, pp. S601-S618.

[10]. D. F. Plusquellic, K. Iegrist, E. J. Heilweil, and Okan Esenturk, Application of Terahertz Spectroscopy in Biosystems, *Chemphyschem*, Vol. 8. 2007, pp. 2412-2431.

[11]. A. J. Fitzgerald, E. Berry, N. N. Zinovev, G. C. Walker, M. A. Smith, and J. M. Chamberlain, An introduction to medical imaging with coherent terahertz frequency radiation, *Phys. Med. Biol*., Vol. 47, 2002,

pp. R67-R84.
[12].T. Nakagawa and H. Murakami, Mid- and far-infrared astronomy mission SPICA, *Adv. Space Res*., Vol. 40, 2007, pp. 679-683.
[13].J. W. Waters, L. Froidevaux, R. S. Harwood, R. F. Jarnot, H. M. Pickett, W. G. Read *et al*., The earth observing system microwave limb sounder (EOS MLS) on the Aura satellite, *IEEE Trans. Geosci. Remote Sensing*, Vol. 44, No. 5, 2006, pp. 1075-1092.
[14].K. Kawase, Y. Ogawa, Y. Watanabe, and H. Inoue, Non-destructive terahertz imaging of illicit drugs using spectral fingerprints, *Opt. Express*, Vol. 11, Issue 20, 2003, pp. 2549-2554.
[15].R. Piesiexicz, M. Jacob, M. Koch, J. Schoebel, and T. Kürner, Performance analysis of future multigigabit wireless communication system at THz frequencies with highly directive antennas in realistic indoor environments, *IEEE J. Selec. Top. Quant. Electron*., Vol. 14, Issue 2, 2008, pp. 421-430.
[16].S. Komiyama, O. Astavief, V. Antonov, T. Kutsuwa, and T. Hirai, A single-photon detector in the far-infrared range, *Nature,* Vol. 403, 2000, pp. 405-407.
[17].O. Astavief, S. Komiyama, T. Kutsuwa, V. Antonov, Y. Kawaguchi, and K. Hirakawa, Single-photon detector in the microwave range, *Appl. Phys. Lett*., Vol. 80, No. 22, 2002, pp. 4250-4252.
[18].H. Hashiba, V. Antonov, L. Kulik, A. Tzalenchuk, P. Kleinschmid, Giblin, and S. Komiyama, Isolated quantum dot in application to terahertz photon counting, *Phys. Rev. B.,* Vol. 73, Issue 8, 2006, pp. 081310.
[19].K. Ikushima. Y. Yoshimura, T. Hasegawa, S. Komiyama, T. Ueda, and K. Hirakawa, Photon counting microscopy of terahertz radiation, *Appl. Phys. Lett*., Vol. 88, Issue 15, 2006, pp. 152110.
[20].K. Ikushima, H. Sakuma, Y. Yoshimura, S. Komiyama, T. Ueda, and K. Hirakawa, THz imaging of cyclotron emission in quantum Hall conductors, *Physica E*, Vol. 34, Issues 1-2, 2006, pp. 22-26.
[21].K. Ikushima, S. Komiyama, T. Ueda, and K. Hirakawa, THz-photon generation due to electrons injected via quantum – Hall edge channels, *Physica E*, Vol. 40, Issue 5, 2008, pp. 1026-1029.
[22].K. Ikushima, D. Asaoka, S. Komiyama, T. Ueda, and K. Hirakawa, Manipulating terahertz photons on a quantum Hall effect device, *Physica E*, Vol. 42, Issue 4, 2010, pp. 1034-1037.
[23].Z. An, J. C. Chen, T. Ueda, S. Komiyama, and K. Hirakawa, Infrared phototransistor using capacitively coupled two-dimensional electron gas layers, *Appl. Phys. Lett*., Vol. 86, Issue 17, 2005, pp. 172106.
[24].Z. An, T. Ueda, J. C. Chen, S. Komiyama, and K. Hirakawa, A sensitive double-quantum well infrared phototransistor, *J. Appl. Phys.,* Vol. 100, Issue 4, 2006, pp. 044509.
[25].Z. An, T. Ueda, S. Komiyama, and K. Hirakawa, Metastable excited states of a closed quantum dot with high sensitivity to infrared photons, *Phys. Rev. B*, Vol. 75, Issue 8, 2007, pp. 085417.
[26].Z. An, T. Ueda, S. Komiyama, and K. Hirakawa, Reset operation of quantum-well infrared phototransistors, *IEEE Trans. Electron Devices*, Vol. 54, No. 7, 2007, pp. 1776-1780.
[27].T. Ueda, Z. An, S. Komiyama, and K. Hirakawa, Charge-sensitive infrared phototransistors: characterization by an all cryogenic spectrometer, *J. Appl. Phys*., Vol. 103, Issue 9, 2008, pp. 093109.
[28].T. Ueda, S. Komiyama, Z. An, N. Nagai, and K. Hirakawa, Temperature dependence of the performance of charge-sensitive infrared phototransistors, *J. Appl. Phys.,* Vol. 105, Issue 6, 2009, pp. 064517.
[29].P. Nickels, S. Matsuda, T. Ueda, Z. An and S. Komiyama, Metal hole arrays as resonant photo-coupler for charge sensitive infrared phototransistors, *IEEE J. Quantum Electronics*, Vol. 46, Issue 3, 2010, pp. 384-389.
[30].J. Yao, K. K. Choi, D. C. Tsui, Optimization of high detectivity infrared hot-electron transistors at low temperature, *IEEE Trans. Electron Devices*, Vol. 48, Issue 7, 2001, pp. 1318-1321.
[31].Y. Kajihara, S. Komiyama, P. Nickels, T. Ueda, Passive long-wavelength infrared microscope with a highly sensitive detector, *Rev. Sci. Instrum*., Vol. 80, 2009, 063702.
[32].Y. Kajihara, K. Kosaka, and S. Komiyama, A sensitive near-field microscope for thermal radiation, *Rev. Sci. Instrum*., Vol. 81, 2010, 033706.

___

Guide for Contributors

Aims and Scope

Sensors & Transducers Journal (ISSN 1726-5479) provides an advanced forum for the science and technology of physical, chemical sensors and biosensors. It publishes state-of-the-art reviews, regular research and application specific papers, short notes, letters to Editor and sensors related books reviews as well as academic, practical and commercial information of interest to its readership. Because it is an open access, peer review international journal, papers rapidly published in *Sensors & Transducers Journal* will receive a very high publicity. The journal is published monthly as twelve issues per annual by International Frequency Association (IFSA). In additional, some special sponsored and conference issues published annually. *Sensors & Transducers Journal* is indexed and abstracted very quickly by Chemical Abstracts, IndexCopernicus Journals Master List, Open J-Gate, Google Scholar, etc.

Topics Covered

Contributions are invited on all aspects of research, development and application of the science and technology of sensors, transducers and sensor instrumentations. Topics include, but are not restricted to:

- Physical, chemical and biosensors;
- Digital, frequency, period, duty-cycle, time interval, PWM, pulse number output sensors and transducers;
- Theory, principles, effects, design, standardization and modeling;
- Smart sensors and systems;
- Sensor instrumentation;
- Virtual instruments;
- Sensors interfaces, buses and networks;
- Signal processing;
- Frequency (period, duty-cycle)-to-digital converters, ADC;
- Technologies and materials;
- Nanosensors;
- Microsystems;
- Applications.

Submission of papers

Articles should be written in English. Authors are invited to submit by e-mail editor@sensorsportal.com 8-14 pages article (including abstract, illustrations (color or grayscale), photos and references) in both: MS Word (doc) and Acrobat (pdf) formats. Detailed preparation instructions, paper example and template of manuscript are available from the journal's webpage: http://www.sensorsportal.com/HTML/DIGEST/Submition.htm Authors must follow the instructions strictly when submitting their manuscripts.

Advertising Information